ACS APPLIED MATERIALS & INTERFACES

Research Article

www.acsami.org

Accelerating the Controlled Synthesis of Metal–Organic Frameworks by a Microfluidic Approach: A Nanoliter Continuous Reactor

Lorena Paseta, Beatriz Seoane, Daniel Julve, Víctor Sebastián, Carlos Téllez, and Joaquín Coronas*

Chemical and Environmental Engineering Department and Instituto de Nanociencia de Aragón (INA), Universidad de Zaragoza, 50018 Zaragoza, Spain

Supporting Information

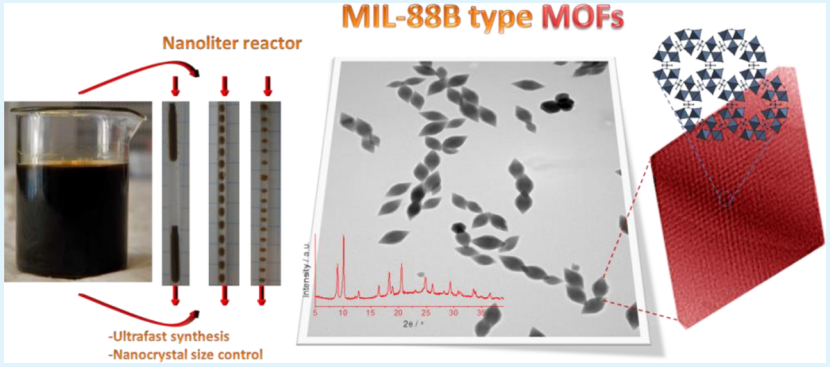

ABSTRACT: Segmented microfluidics was applied to the ultrafast crystallization of dicarboxylate based MIL-88B type metal–organic frameworks (MOFs; Fe-MIL-88B-NH_2, Fe-MIL-88B, and Fe-MIL-88B-Br). Particular attention was paid to the influence of the temperature, residence time, and slug volume on the size and crystal size distribution of the MOFs. Average sizes in the 90–900 nm range with relatively narrow crystal size distributions were obtained with residence times as short as 20 s depending on the MOF type and synthesis conditions.

KEYWORDS: *segmented microfluidics, continuous synthesis, metal–organic framework, dicarboxylate, MIL-88B*

INTRODUCTION

In the search for new metal-organic framework (MOF) materials and also for synthesis control to achieve required physicochemical properties, a number of synthetic techniques have been proposed beyond solvothermal synthesis. Ultrasound[1] and microwave-assisted[2] crystallization render crystal size control and reduce synthesis time. Ionothermal synthesis uses the same ionic liquid compound as both solvent and ligand.[2] Electrosynthesis of MOFs leads to fast surface coating.[3] Mechanochemical synthesis by ball milling has also been reported as a simple and green method working in the absence of solvent.[4] In addition to these consolidating techniques for obtaining MOFs, a few examples can be found related to the use of continuous systems[5] and even of microfluidics.[6] In particular, 375 μm diameter hollow capsules of $[Cu_3(BTC)_2]$ have been prepared by co-flowing a metal containing aqueous phase together with a ligand organic solution in a 0.76 mm ID tube,[6a] while the microfluidic high-throughput has been used for fabricating MOF single crystal arrays,[6b] a MOF has been moved within a microfluidic circuit by means of a magnetic field,[6c] and MOF patters have been generated through digital microfluidics.[6d,e] Despite the potential of microfluidics for establishing new synthetic routes toward MOFs[7] and the clear advantages of this methodology (residence time control, heat and mass transport enhancement, etc.),[8] the number of related studies is scarce.

MIL-88, with chemical composition $M^{III}_3O(L)_3\cdot(H_2O)_2\cdot X$ with M = Fe or Cr,[9] or Sc,[10] L = linear dicarboxylate, and X = anion, is composed of trimeric metal octahedral units (three metallic octahedral FeO_6 shared by μ_3O). These units are interconnected by the organic linker to form two types of pores: bipyramidal cages delimited by five trimers at the vertices and six dicarboxylate groups, and narrow hexagon channels along the *c* axis delimited by six trimers whose vertices are the central μ_3O atoms.[9] Depending on the length of the organic ligand used, there are different isoreticular members of the MIL-88 family: MIL-88A (cell volume 1500 Å^3), MIL-88B (cell volume 1980 Å^3), MIL-88C (cell volume 2020 Å^3), and MIL-88D (cell volume 3500 Å^3) containing fumaric, terephthalic, 2,6-naphthalenedicarboxylic, and 4,4′-biphenyldicarboxylic acids, respectively.[9b] MIL-88 presents the largest expansion ever evidenced for a crystalline hybrid solid with an increase in cell volume up to 230%, for Cr-MIL-88D, upon breathing in polar solvents such as pyridine with reversible atomic displacements up to 10 Å.[11] This framework flexibility makes

Received: April 24, 2013
Accepted: September 13, 2013
Published: September 13, 2013

   dx.doi.org/10.1021/am4029872 | ACS Appl. Mater. Interfaces 2013, 5, 9405–9410

MIL-88 a good candidate for adsorption of different organic molecules[9c] or for sensors. Besides, Fe(III) dicarboxylate MOFs exhibit interesting properties in biomedical application such as drug delivery or imaging.[12]

The main approaches to obtain zero-dimensional nanostructures are, besides traditional discontinuous systems (i.e. round bottom flask) and direct precipitation,[13] microwave-assisted synthesis, ultrasound treatment, microemulsion-based synthesis, and interfacial synthesis.[14] Spray drying enables assembling of MOF nanoparticles in 5 μm hollow spheres, whose disaggregation by sonication produces discrete nanoparticles.[15] However, microfluidic systems have been reported to allow a good control of the particle size and morphology together with a good reproducibility.[14] In this respect, we believe that the systematic study of different MOFs under different conditions using a microfluidic system could lead to a new robust approach to control particle size with high reproducibility. This article deals with the application of segmented flow in microfluidics[16] to the synthesis of dicarboxylate based MIL-88B type MOFs: Fe-MIL-88B-NH_2, Fe-MIL-88B, and Fe-MIL-88B-Br designated along the paper as NH_2, 4H, and Br, respectively. Flow segmentation in discrete slugs promotes the internal circulation; in consequence it generates uniformly sized nanoparticles resulting from the rapid mixing and efficient mass and heat transfer.[8] Furthermore, the use of segmented liquid–liquid flow can prevent the particles from interacting with the reactor walls and therefore minimize reactor clogging. The influence of the residence time and temperature conditions on the particle size distribution was studied for these three MOFs. Particle size distribution control is of paramount importance when, inter alia, adsorption,[17] catalysis,[18] sensor,[19] magnetic resonance imaging,[20] coating,[21] and mixed matrix membrane[22] applications are addressed.

EXPERIMENTAL SECTION

Synthesis of MOFs. For the microfluidic system (Figure 1), three syringe pumps (NE-300, New Era Pump Systems) were connected by

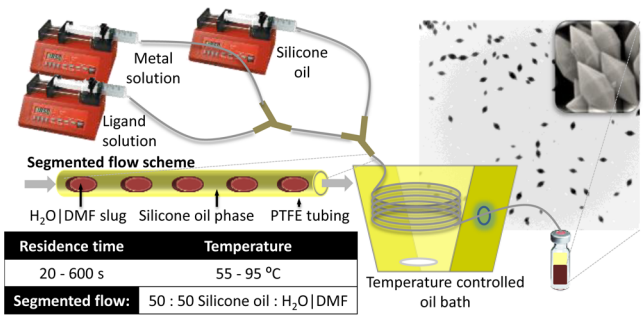

Figure 1. Schematic of the microfluidic setup, segmented flow pattern, and synthesis details. Both reactants and silicone oil streams were of the same value (in the 60–600 μL/min range), so that residence times in the 20–600 s range were achieved.

means of Teflon tubing (0.04 in. i.d. and 1/16 in. o.d.) to combine two reactant streams with a silicone oil (350 CST, Manuel Riesgo SA) stream. Both reactants and silicone oil streams were of the same value (in the 60–600 μL/min range), so that using 20 mL polypropylene syringes (Sigma Aldrich, ref 305617) and a reactor length of 1.5 m (which corresponds to a 1.2 cm^3 volume), residence times (calculated as the volume to total flow ratio, including silicone oil) in the 20–600 s range were achieved. The molar compositions corresponding to all the experiments carried out here are shown in Supporting Information Table S1. Besides the advantages of segmented flow, the use of silicone oil prevented from reactor plugging and particle aggregation, so that experiments without its use were not feasible.

In a typical synthesis of Fe-MIL-88B-NH_2 (NH_2), two different solutions were prepared. First, 4.0 mmol (1.080 g) of $FeCl_3{\cdot}6H_2O$ (Sigma Aldrich, ≥98%) was dissolved in a mixture of 3.8 mL of distilled H_2O and 6.2 mL of *N*,*N*-dimethylformamide (DMF, Alfa Aesar). Second, 4.0 mmol (0.720 g) of NH_2–H_2BDC (2-amino-benzene-1,4-dicarboxylic acid, Sigma Aldrich, 99%) was added to 10 mL of DMF and stirred until a clear solution was obtained. Both solutions were transferred to respective syringes and injected by means of two syringe pumps into the mixing-cold zone of the reactor. A third syringe pump injected silicone oil as discrete droplets into the synthesis gel giving rise to a segmented flow. In addition, silicone oil flowing along the wall of the tube avoided the deposition of MOF particles. The segmented flow was introduced into the reaction-hot zone which was heated using a silicon bath set at 55, 75, or 95 °C depending on the experiment. Residence times ranging from 60 to 600 s were tuned according to the modification of the total flow rates, keeping the microreactor volume and the silicone oil/aqueous phase rate constant. Experiments with a residence time under 60 s were carried out at a constant flow rate but modifying accordingly the reactor volume.

To obtain Fe-MIL-88B (4H), 4.0 mmol (1.080 g) of $FeCl_3{\cdot}6H_2O$ was dissolved in 3.8 mL of water and 6.2 mL of DMF solution, and 2.8 mmol (0.465 g) of H_2BDC (benzene-1,4-dicarboxylic acid, Sigma Aldrich, 98%) was dissolved in 10 mL DMF. Both solutions were loaded into different syringe pumps and injected as segmented flow into the reaction-hot zone at 95 °C for 4 min.

In the case of Fe-MIL-88B-Br (Br), the synthesis gel was more diluted (Supporting Information Table S1) and was prepared as follows: 2.0 mmol (0.540 g) of $FeCl_3{\cdot}6H_2O$ was dissolved in a mixture of 3.8 mL of water and 6.2 mL of DMF, while 2.0 mmol (0.500 g) of Br–H_2BDC (2-bromobenzene-1,4-dicarboxylic acid, Sigma Aldrich, 95%) was added to 10 mL of DMF. At 95 °C the minimum synthesis time needed was 6 min.

For all the three MOFs the synthesis gel was collected in a glass vial at 0 °C and two immiscible phases were formed: the H_2O/DMF mixture with the dispersed MOF particles at the bottom and the silicon oil at the top. The bottom, aqueous phase was recovered with a syringe, centrifuged (at 10 000 rpm for 10 min), and washed with acetone.

After drying at room temperature, the powders were activated according to the following procedures at room temperature. Fe-MIL-88B-NH_2 (200 mg) was stirred with 15 mL DMF for 1 h, washed with ethanol three times, and dried at 100 °C overnight. Fe-MIL-88B (200 mg) was stirred with 100 mL of deionized water for 12 h; after centrifugation, the sample was dried at room temperature. Fe-MIL-88B-Br (200 mg) was dispersed in 50 mL of DMF and stirred for 2 h, centrifuged and washed with ethanol to remove the DMF; finally, the sample was dried overnight at 150 °C under vacuum.

Characterization. Powder X-ray diffraction (XRD) was performed at room temperature in a D-Max Rigaku diffractometer with a copper anode and a graphite monochoromator so as to select Cu–Kα_1 radiation (λ = 1.5418 Å). Data were collected in the 2.5–40° 2θ range, and the scanning rate used was 0.03°/s. FullProf software was used to indexate some selected samples. Before acquiring the XRD patterns the samples were kept for 3 h under moisture to obtain the hydrated forms comparable to the simulated data.

Thermogravimetric analyses (TGA) were performed using a TGA/SDTA 851e system (Mettler Toledo). The samples were heated up to 850 °C with a heating rate of 10 °C/min under an air flow of 80 cm^3(STP)/min.

Powder samples were characterized by infrared spectroscopy (FTIR) preparing MOF-KBr pills, and the spectra were collected from 4000 to 400 cm^{-1} with a Shimadzu IRAffinity spectrometer with a resolution of 4 cm^{-1}.

Transmission electron microscopy (TEM) and cryo-TEM images were taken with a FEI Tecnai T20 microscope at 200 kV. To prepare samples for TEM observation, 1.5 mL synthesis gel was recovered with a syringe at the exit of the reactor from the above-mentioned bottom

dx.doi.org/10.1021/am4029872 | ACS Appl. Mater. Interfaces 2013, 5, 9405–9410

aqueous phase. This was transferred to another vial, centrifuged and washed with ethanol, and the obtained solid was suspended in 5 mL ethanol. After 2 min in an ultrasonic bath, a drop of this suspension was applied to a copper grid (200 mesh) coated with carbon film, and allowed to dry in air. In the case of the cryo-TEM samples, MOF nanocrystal suspension was vitrified just after sample collection in the microfluidic set-up in an automated vitrification robot (FEI Vitrobot) using liquid ethane. The TEM grids were transferred to a cryo workstation and then into a cryo-holder. Taking into account their largest dimension, the crystal sizes were assessed using DigitalMicrograph software.

RESULTS AND DISCUSSION

Even though most segmented microfluidic experiments (Figure 1) were carried out with NH_2−H_2BDC (2-aminobenzene-1,4-dicarboxylic acid), two other ligands, H_2BDC (benzene-1,4-dicarboxylic acid), and Br−H_2BDC (2-bromobenzene-1,4-dicarboxylic acid), were studied to increase the breadth of our findings. As shown in Figure 2, the XRD patterns of the

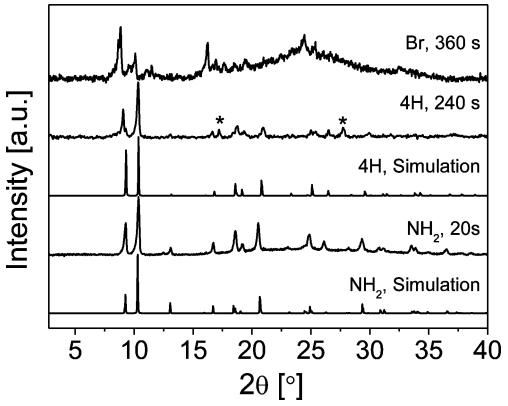

Figure 2. XRD patterns of Fe-MIL-88B-NH_2 (95 °C, 20 s), Fe-MIL-88B (95 °C, 4 min), and Fe-MIL-88B-Br (95 °C, 6 min). Simulated XRD patterns are also shown. The wavelength used for both experimental and simulated patterns was Cu Kα radiation (λ = 1.5418 Å). The peaks observed for Fe-MIL-88B at 17.2 and 27.8° are due to non-encapsulated terephthalic acid.

products obtained are consistent with those simulated with Diamond software from CIF archives for Fe-MIL-88B-NH_2[23] and the Cr analogous Cr-MIL-88B.[9b] Furthermore, the XRD patterns in Figure 2 were indexed and the cell parameters together with the corresponding cell volumes are shown in Supporting Information Table S2. The offset between the experimental and the theoretical MIL-88B-Br XRD pattern lead to an increase in the cell parameters *a* and *b* compared to the simulated dry form[24] and a decrease in *c* with the concomitant increase in the cell volume. We suggest that this is due to the fact that the structure was partially open due to the bulky functional group of the ligand. Fe-MIL-88B-NH_2, Fe-MIL-88B, and Fe-MIL-88B-Br were obtained at 95 °C after 20 s, 4 min, and 6 min, respectively, while the reported milder conditions for these materials are 24 h at 110 °C in water,[25] 12 h at 100 °C, and 12 h at 100 °C, both in DMF,[24] respectively. Very short synthesis times have been reported when segmented microfluidics was applied to zeolites A[26] and ZSM-5.[27] As will be corroborated throughout the study, the microfluidic approach considerably accelerates the synthesis of MIL-88B based MOFs, leading to crystals clearly below 1 μm (average values of 180, 520, and 680 nm for Fe-MIL-88B-NH_2, Fe-MIL-88B, and Fe-MIL-88B-Br, respectively) with narrow particle size distributions (Figure 3) and after very short residence times (20 s). It is worth mentioning that to prepare Fe-MIL-

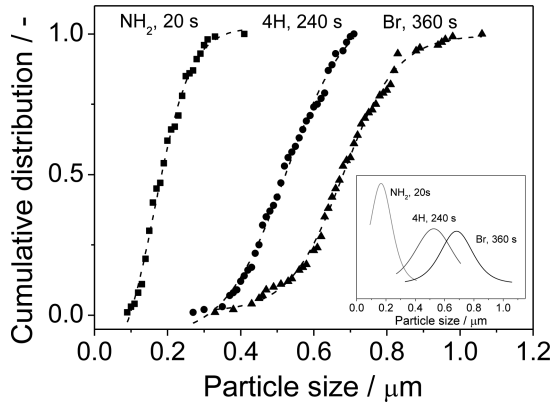

Figure 3. Cumulative particle size distribution of Fe-MIL-88B-NH_2 (95 °C, 20 s), Fe-MIL-88B (95 °C, 4 min), and Fe-MIL-88B-Br (95 °C, 6 min). Dashed lines correspond to the fitting to a Boltzmann equation, with first derivatives in the inset.

88B and MIL-88B-Br longer times are needed (4 and 6 min versus 20 s) leading to more polydispersed and larger particle sizes. It is likely that decreasing the temperature and reaction time may lead to amorphous phases.

Particles as small as 200 nm or below were already reported by Chalati et al.[28] for the MIL-88 topology. Fe-MIL-88A with particle sizes below 200 nm were obtained under mild solvothermal (DMF or methanol) or hydrothermal conditions, using ultrasound treatment in water at 0 and 20 °C and with microwave irradiation. Just in the latter case 195 ± 15 nm particles with 51 ± 1 % yield.[28] Although in the microwave-assisted synthesis of Fe-MIL-88A the particle size was smaller and the particle size distribution narrower; the synthesis reported here is faster (20 s compared to 30 min), and the crystallinity clearly higher. However, our yields were in the 0.6−12.4 % range, depending on the synthesis conditions (Supporting Information Table S1). Other synthetic approach to obtain nanoparticles with controlled size and aspect ratios of Fe-MIL-88B-NH_2 used simultaneously the triblock copolymer F127 and acetic acid.[25] In this case nanoparticles with high yield could be obtained but the synthesis was much longer (24 h) and the crystallinity lower than that reported here.

Before continuing with the discussion of the results, a comment should be made on the way in which the reaction was stopped and the samples prepared for TEM observation. Separated from the silicone oil, the synthesis dispersion with MOF crystals and non-converted reactants was diluted in ethanol and centrifuged several times before being placed on the TEM grid. To check that this handling did not alter the size of the particles obtained, the synthesis dispersion was directly observed by cryo-TEM without the described processing. Figure 4 shows that, despite the slightly larger size of crystals observed by TEM which suggest that the reaction continued a little bit during the purification process, the particle size distributions are in practice similar in both cases, concluding that the method used to obtain crystals for characterization is reliable.

Microfluidics not only enabled ultrafast synthesis of the MOFs but also control of the particle size distribution. As demonstrated for Fe-MIL-88B-NH_2, Figure 5 shows a continuous increase in particle size (from average values of

dx.doi.org/10.1021/am4029872 | ACS Appl. Mater. Interfaces 2013, 5, 9405−9410

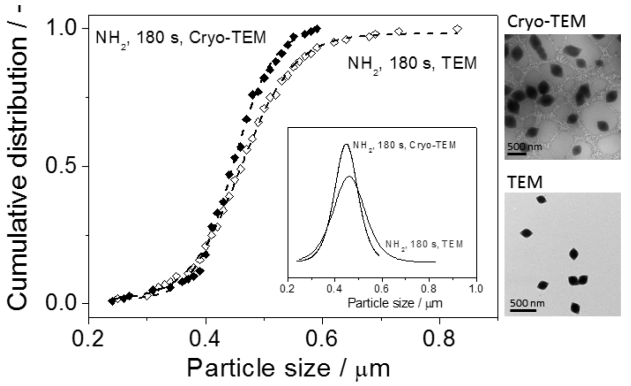

Figure 4. Cumulative particle size distribution of Fe-MIL-88B-NH_2 (95 °C, 180 s) from cryo-TEM and conventional TEM (see examples of images on the right). Dashed lines correspond to the fitting to a Boltzmann equation, with first derivatives shown in the inset.

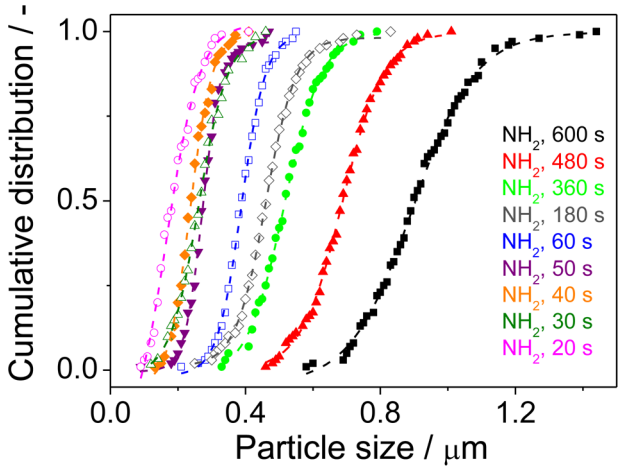

Figure 5. Cumulative particle size distribution of Fe-MIL-88B-NH_2 synthesized at 95 °C after several residence times. Dashed lines correspond to the fitting to a Boltzmann equation.

180 to 900 nm) as a function of residence time (from 20 to 600 s) and also a clear augmentation of the dispersion of the distributions. The crystal sizes were measured from TEM images like those in Figure 6, showing that the growth habit definition from round to more angular shaped particles runs parallel to their enlargement. Both the increase in particle size and the decrease in distribution narrowness are more evident in Figure 7, where the standard deviation of the predominant sizes (obtained from maxima of derivatives from cumulative curves in Figure 5) clearly increased at residence times above 400 s. As the residence time increased (from 20−60 to 600 s), so did the slug length (from 0.8 to 8.5 mm) giving rise to considerably larger slug volumes (from 100 nL to 1.7 μL). Supporting Information Figure S1 shows XRD patterns for selected Fe-MIL-88B-NH_2 samples (obtained at 20, 40, 60, 360, and 600 s), all of them in agreement with the simulated pattern.

A final comparison arose from Supporting Information Figure S2 where average sizes of 2.1 and 0.90 μm are observed for discontinuous (see Supporting Information Figure S3 for the SEM appearance), and continuous experiments, respectively, carried out in the same conditions of 600 s of residence time and 95 °C. This allows one to verify once more the suitability of our approach.

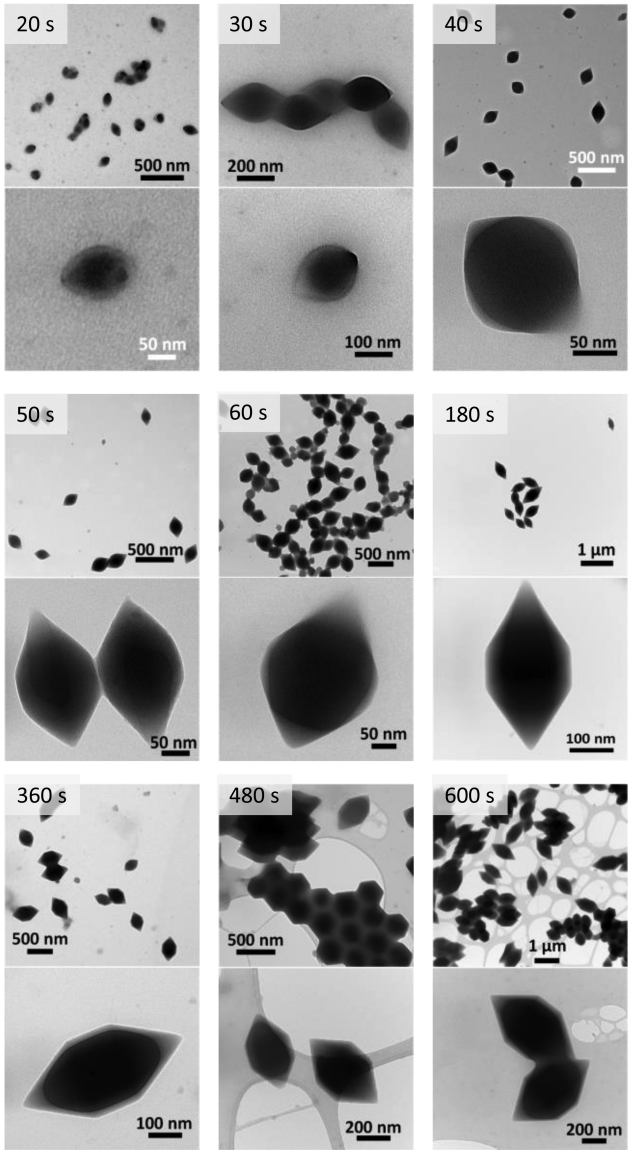

Figure 6. TEM images of Fe-MIL-88B-NH_2 synthesized at 95 °C after several residence times.

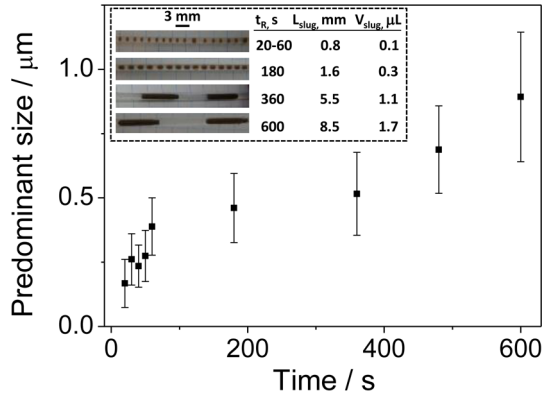

Figure 7. Predominant sizes corresponding to the particle size distributions shown in Figure 5 for Fe-MIL-88B-NH_2. The inset shows the slug details for the different residence times used.

The most interesting achievement of the microfluidic reactor selected here to synthesize MOFs, where the oil phase is the

dx.doi.org/10.1021/am4029872 | ACS Appl. Mater. Interfaces 2013, 5, 9405−9410

continuous phase, is that the non-miscible, aqueous (water/DMF) phase is dispersed into nanoscale volume segments. Thus, axial dispersion is greatly reduced, and individual aqueous segments or slugs act like disconnected stirred vessels with no communication between them. The configuration of alternating slugs of two liquid phases provides a unique environment for improving mass transfer and reaction within the microreactor under a laminar regime.[16] In the absence of flow segmentation (laminar flow pattern), the concentration gradient is axial and the mass transfer occurs across an area corresponding to the channel cross section and over a path length equal to half the length of the channel width, assuming that volumetric feed ratios into a mixing junction are approximately equal. Nevertheless, under a segmented flow, an internal circulation is generated within the slugs, which is stimulated by the shear between the continuous phase at the capillary wall and the slug. The velocity difference between the two immiscible phases and the slug length governs the internal circulation in the slug and hence the particle size distribution, while it has been found that the strength of the recirculation, characterized by the vorticity, increases with decreasing residence time and slug length.[16] Then, it seems reasonable that under a residence time of 60 s, where the slug length did not vary because the reactor volume was modified against reactant flow to preserve the slug stability, the MOF nanocrystal size evolved according to the inherent crystallization kinetics, obtaining the smallest nanocrystals at 20 s (190 nm). At higher residence times, where the flow rates decreased, the aqueous slug length increased from 0.8 to 8.5 mm, at 60 and 600 s, respectively. This implies that at residence times below 60 s the slug volume was 100 nL, while at a residence time of 600 s the slug volume increased to 1.7 μL. Consequently, the interphase region affected by vorticity was notably decreased, influencing the mixing in the water/DMF slug and broadening the size distribution as the residence time increased from 60 to 600 s (Figure 7).

These findings are in full agreement with previous results relating to nanocrystal synthesis in segmented microfluidics.[16,29] Finally, from the results obtained it can also be inferred that at long residence times the segmented microreactor performance tends to be similar to that of a batch reactor where the poor mixing strongly effects the particle size distribution of fast kinetic crystallizations.

An additional result that highlights the flexibility of our system concerns its temperature performance. As Supporting Information Figure S4 illustrates, temperature exerts a strong effect on the MOF growing rate and, consequently, on both average size (90, 180, and 390 nm at 55, 75, and 95 °C, respectively) and distribution narrowness, which improves with decreasing temperature. Note that the crystal size distribution control exhibited in the present study was achieved at the highest temperature tested of 95 °C, which inherently widens the distribution (Supporting Information Figure S4, inset).

An insight into the application of these materials is given by their activation by solvent exchange with DMF/ethanol and water for Fe-MIL-88B-Br and Fe-MIL-88B-NH_2, and Fe-MIL-88B, respectively. This was effectively carried out as described in the Experimental Section; however, it is worth mentioning that the water treatment may hydrolyze the materials, as Supporting Information Figure S5 suggests after 12 h of treatment under moisture, the Br-form MOF being the most affected. The corresponding weight loss curves of the activated materials (Supporting Information Figure S6) show only low temperature remains of solvent. Besides, these curves suggest that the materials may be thermally stable until about 300 °C, the stability increasing from Fe-MIL-88B to Fe-MIL-88B-NH_2 and from this to Fe-MIL-88B-Br with maximum weight loss temperatures of 296, 308, and 365 °C, respectively. According to the weight losses observed and taking into account the spectra obtained by FTIR spectroscopy (see below), the empirical formulae could be calculated as $Fe^{III}_3O(L)_3\cdot(H_2O)_2\cdot X\cdot nH_2O$ where X is Cl^- and n = 5.6, 7.8, and 5.3 for Fe-MIL-88B-NH_2, Fe-MIL-88B, and Fe-MIL-88B-Br, respectively. It is worth mentioning that no clear effect on thermal behavior was observed as a function of particle size; in fact, Supporting Information Figure S7 shows TGA curves for as-made Fe-MIL-88B-NH_2 materials prepared at 40, 360, and 600 s (i.e. with average sizes obtained from Figure 5 of 0.24, 0.52, and 0.90 μm, respectively) where the observed discrepancies may be due to small amounts of remaining reagents.

Additionally, these materials were characterized by FTIR spectroscopy (Figure 8). The signals at 3461 and 3335 cm^{-1} for

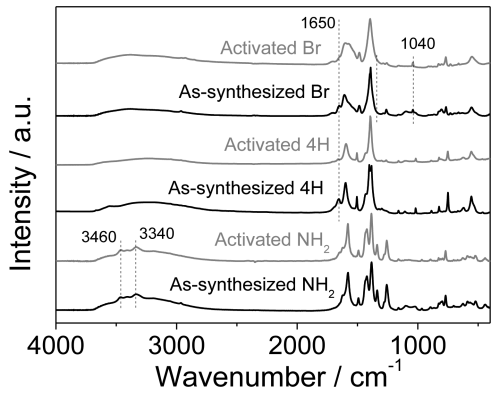

Figure 8. FTIR sepectra of as-synthesized and activated Fe-MIL-88B-NH_2 (95 °C, 20 s), Fe-MIL-88B (95 °C, 4 min), and Fe-MIL-88B-Br (95 °C, 6 min).

the activated and as-synthesized Fe-MIL-88B-NH_2 correspond to the asymmetric and symmetric stretching absorption of primary amine groups,[30] while the peak at 1040 cm^{-1} corresponds to the presence of brominated aromatic compounds. The absence of a band at 1678 or at 1656 cm^{-1}, corresponding to the C═O stretching vibration of the protonated NH_2−H_2BDC and the carbonyl group of the DMF, respectively, indicated that the as-synthesized Fe-MIL-88B-NH_2 was already activated and only water molecules would be trapped inside its pores after the synthesis. However, a signal at 1656 cm^{-1} due to the C═O of the DMF was observed for as-synthesized Fe-MIL-88B and Fe-MIL-88B-Br indicating that DMF molecules were inside its pores. This signal vanished upon the successful activation carried out here.

The possible adsorption of silicone oil on the as-synthesized MOFs was discarded from FTIR analysis where the 2965 cm^{-1} intensity corresponding to CH stretching of silicone oil methyl groups was not observed, even though we cannot rule out the superficial adsorption of a small amount of the oil on the MOF.

Finally, only some modified MIL-88B structures possess a permanent porosity including the CH_3, $2CH_3$, $4CH_3$, and $2CF_3$ functionalized solids, while others (including those studied here) do not show accessibility for N_2.[24] This is the reason why the N_2 adsorption was omitted here; nevertheless, these materials can absorb ethanol, toluene, or pyridine.[24]

dx.doi.org/10.1021/am4029872 | ACS Appl. Mater. Interfaces 2013, 5, 9405−9410

CONCLUSIONS

The feasibility of applying the segmented flow microfluidic approach to the crystallization of MIL-88B MOFs with three different ligands (i.e. this methodology has been applied to three different MOFs) has been demonstrated. A fine tuning of the crystal size and the narrowness of the crystal size distribution was achieved as a function of residence time (as short as 20 s) and volume slug (as small as 100 nL). Additionally, it has been shown that a higher slip velocity yields a narrow particle size distribution, while a lower slip velocity leads to a poor internal mixing in the slugs, which in turn widens the particle size distribution.

Furthermore, given the short duration of the synthesis and the small amount of reagents involved, future studies will demonstrate whether the microfluidic methodology can provide a useful tool for the general control of shape, size and functionality of MOFs. Even though microfluidics presents some limitation related to the low yield, due to the reliable results obtained here, we believe that this methodology could be applied to other families of MOFs.

ASSOCIATED CONTENT

Supporting Information

Summary of synthesis conditions and yields. Crystallographic parameters of selected samples. Complementary XRD patterns for selected Fe-MIL-88B-NH_2 samples obtained at different residence times. Comparison between continuous and discontinuous synthesis results. Cumulative particle size distribution of Fe-MIL-88B-NH_2 at 55, 75, and 95 °C. XRD patterns of materials after moisture exposure. TGA curves of as-made and activated materials. This material is available free of charge via the Internet at http://pubs.acs.org.

AUTHOR INFORMATION

Corresponding Author

*E-mail: coronas@unizar.es.

Notes

The authors declare no competing financial interest.

ACKNOWLEDGMENTS

Financial support from the Spanish Ministry of Economy and Competitiveness (MAT2010-15870 and FPU Program fellowship for B.S.), the Aragón Government, the ESF, and the People Program (Marie Curie Actions) of the EU under REA grant agreement no. 321642 are gratefully acknowledged.

REFERENCES

(1) Seoane, B.; Zamaro, J. M.; Tellez, C.; Coronas, J. *CrystEngComm* **2012**, *14*, 3103−3107.
(2) Lin, Z. J.; Wragg, D. S.; Morris, R. E. *Chem. Commun.* **2006**, 2021−2023.
(3) Li, M. Y.; Dinca, M. *J. Am. Chem. Soc.* **2011**, *133*, 12926−12929.
(4) Klimakow, M.; Klobes, P.; Thunemann, A. F.; Rademann, K.; Emmerling, F. *Chem. Mater.* **2010**, *22*, 5216−5221.
(5) (a) Schoenecker, P. M.; Belancik, G. A.; Grabicka, B. E.; Walton, K. S. *AIChE J.* **2013**, *59*, 1255−1262. (b) Garcia Marquez, A.; Horcajada, P.; Grosso, D.; Ferey, G.; Serre, C.; Sanchez, C.; Boissiere. *Chem. Commun.* **2013**, *49*, 3484−3850.
(6) (a) Ameloot, R.; Vermoortele, F.; Vanhove, W.; Roeffaers, M. B. J.; Sels, B. F.; De Vos, D. E. *Nature Chem.* **2011**, *3*, 382−387. (b) Witters, D.; Vergauwe, N.; Ameloot, R.; Vermeir, S.; De Vos, D.; Puers, R.; Sels, B.; Lammertyn, J. *Adv. Mater.* **2012**, *24*, 1316−1320. (c) Falcaro, P.; Lapierre, F.; Marmiroli, B.; Styles, M.; Zhu, Y.G.; Takahashi, M.; Hill, A. J. *J. Mater. Chem. C* **2013**, *1*, 42−45. (d) Witters, D.; Vermeir, S.; Puers, R.; Sels, B. F.; De Vos, D. E.; Ameloot, R. *Chem. Mater.* **2013**, *25*, 1021−1023. (e) Witters, D.; Vergauwe, N.; Ameloot, R.; Vermeir, S.; De Vos, D.; Puers, R.; Sels, B.; Lammertyn, J. *Adv. Mater.* **2012**, *24*, 1316−1320.
(7) Flugel, E. A.; Ranft, A.; Haase, F.; Lotsch, B. V. *J. Mater. Chem.* **2012**, *22*, 10119−10133.
(8) Jensen, K. F. *Chem. Eng. Sci.* **2001**, *56*, 293−303.
(9) (a) Serre, C.; Millange, F.; Surble, S.; Ferey, G. *Angew. Chem., Int. Ed.* **2004**, *43*, 6286−6289. (b) Surble, S.; Serre, C.; Mellot-Draznieks, C.; Millange, F.; Ferey, G. *Chem. Commun.* **2006**, 284−286. (c) Ramsahye, N. A.; Trung, T. K.; Scott, L.; Nouar, F.; Devic, T.; Horcajada, P.; Magnier, E.; David, O.; Serre, C.; Trens, P. *Chem. Mater.* **2013**, *25*, 479−488.
(10) Mowat, J. P. S.; Miller, S. R.; Slawin, A. M. Z.; Seymour, V. R.; Ashbrook, S. E.; Wright, P. A. *Microporous Mesoporous Mater.* **2011**, *142*, 322−333.
(11) (a) Serre, C.; Mellot-Draznieks, C.; Surble, S.; Audebrand, N.; Filinchuk, Y.; Ferey, G. *Science* **2007**, *315*, 1828−1831. (b) Férey, G.; Serre, C. *Chem. Soc. Rev.* **2009**, *38*, 1380−1399.
(12) (a) Horcajada, P.; Chalati, T.; Serre, C.; Gillet, B.; Sebrie, C.; Baati, T.; Eubank, J. F.; Heurtaux, D.; Clayette, P.; Kreuz, C.; Chang, J. S.; Hwang, Y. K.; Marsaud, V.; Bories, P. N.; Cynober, L.; Gil, S.; Ferey, G.; Couvreur, P.; Gref, R. *Nat. Mater.* **2010**, *9*, 172−178. (b) McKinlay, A. C.; Morris, R. E.; Horcajada, P.; Ferey, G.; Gref, R.; Couvreur, P.; Serre, C. *Angew. Chem. Int. Ed.* **2010**, *49*, 6260−6266. (c) Gaudin, C.; Cunha, D.; Ivanoff, E.; Horcajada, P.; Cheve, G.; Yasri, A.; Loget, O.; Serre, C.; Maurin, G. *Microporous Mesoporous Mater.* **2012**, *157*, 124−130.
(13) Perez, E. V.; Balkus, K. J.; Ferraris, J. P.; Musselman, I. H. *J. Membr. Sci.* **2009**, *328*, 165−173.
(14) Flugel, E. A.; Ranft, A.; Haase, F.; Lotsch, B. V. *J. Mater. Chem.* **2012**, *22*, 10119−10133.
(15) Carne-Sanchez, A.; Imaz, I.; Cano-Sarabia, M.; Maspoch, D. *Nature Chem.* **2013**, *5*, 203−211.
(16) Cabeza, V. S.; Kuhn, S.; Kulkarni, A. A.; Jensen, K. F. *Langmuir* **2012**, *28*, 7007−7013.
(17) Jiang, D. M.; Burrows, A. D.; Edler, K. J. *CrystEngComm* **2011**, *13*, 6916−6919.
(18) Wee, L. H.; Lohe, M. R.; Janssens, N.; Kaskel, S.; Martens, J. A. *J. Mater. Chem.* **2012**, *22*, 13742−13746.
(19) Lu, G.; Farha, O. K.; Kreno, L. E.; Schoenecker, P. M.; Walton, K. S.; Van Duyne, R. P.; Hupp, J. T. *Adv. Mater.* **2011**, *23*, 4449−4454.
(20) Hatakeyama, W.; Sanchez, T. J.; Rowe, M. D.; Serkova, N. J.; Liberatore, M. W.; Boyes, S. G. *ACS Appl. Mater. Interfaces* **2011**, *3*, 1502−1510.
(21) Gascon, J.; Aguado, S.; Kapteijn, F. *Microporous Mesoporous Mater.* **2008**, *113*, 132−138.
(22) Seoane, B.; Zamaro, J. M.; Tellez, C.; Coronas, J. *RSC Adv.* **2011**, *1*, 917−922.
(23) Bauer, S.; Serre, C.; Devic, T.; Horcajada, P.; Marrot, J.; Ferey, G.; Stock, N. *Inorg. Chem.* **2008**, *47*, 7568−7576.
(24) Horcajada, P.; Salles, F.; Wuttke, S.; Devic, T.; Heurtaux, D.; Maurin, G.; Vimont, A.; Daturi, M.; David, O.; Magnier, E.; Stock, N.; Filinchuk, Y.; Popov, D.; Riekel, C.; Ferey, G.; Serre, C. *J. Am. Chem. Soc.* **2011**, *133*, 17839−17847.
(25) Pham, M. H.; Vuong, T.; Vu, A. T.; Do, T. O. *Langmuir* **2011**, *27*, 15261−15267.
(26) Pan, Y.; Yao, J.; Zhang, L.; Xu, N. *Ind. Eng. Chem. Res.* **2009**, *48*, 8471−8477.
(27) Hoang, P. H.; Park, H.; Kim, D.-P. *J. Am. Chem. Soc.* **2011**, *133*, 14765−14770.
(28) Chalati, T.; Horcajada, P.; Gref, R.; Couvreur, P.; Serre, C. *J. Mater.Chem.* **2011**, *21*, 2220−2227.
(29) Kumar, D. V. R.; Prasad, B. L. V.; Kulkarni, A. A. *Chem. Eng. J.* **2012**, *192*, 357−368.
(30) Ahnfeldt, T.; Gunzelmann, D.; Loiseau, T.; Hirsemann, D.; Senker, J.; Ferey, G.; Stock, N. *Inorg. Chem.* **2009**, *48*, 3057−3064.